published in J. Chem. Phys., 113, 5971-5979 (2000)

Do thermotropic biaxial nematics exist? A Monte Carlo study of biaxial Gay–Berne particles.

R. Berardi and C. Zannoni,

Dipartimento di Chimica Fisica e Inorganica,

Università, Viale Risorgimento 4,

40136 Bologna, Italy.

April 11, 2000

Abstract

We have investigated with extensive Monte Carlo simulations in the isothermal isobaric ensemble a system of $N = 8192$ elongated attractive–repulsive biaxial Gay–Berne (GB) particles. We have found a uniaxial and biaxial nematic and a biaxial orthogonal smectic phase in this thermotropic model system.

1 Introduction

Biaxial nematic phases have been a subject of great interest for some time and this interest is increasing as the chase for undisputed thermotropic biaxial nematics continues [1]. Part of this focused attention comes from the possibility of technological applications in the fast display area [2], but much of the fascination of the subject certainly originates from the basic research arena and from the hiatus between theoretical [3] and experimental predictions [4, 5]. Biaxial nematics are not theoretically forbidden and indeed have been predicted to exist, and thus to be the most stable phase in a certain range of thermodynamic conditions, by various approximate theories, mainly on the basis of considerations of orientational order and of orientational free energy [3, 6, 7, 8, 9, 10].

Monte Carlo simulations of systems of interacting biaxial centers placed on a lattice [11, 12] have essentially confirmed these predictions and the phase diagram obtained [12] has shown a biaxial region where the biaxial phase is stable compared to both the uniaxial nematic and isotropic ones. However, as we have already mentioned, none of the low molecular mass thermotropic biaxial nematics put forward [13] appears to have been universally accepted as such. Indeed various of the compounds classified as biaxial nematics on the basis of their optical behavior have shown no detectable biaxiality when examined with deuterium NMR [4, 5]. Such a searching test appears not to have been yet performed on the polymer nematic liquid crystals classified as biaxial [14].

Surprisingly enough the only generally recognized biaxial nematic is the first one to be discovered: the lyotropic system introduced by Yu and Saupe in 1980 [15] although a recent report raises some doubts even on the stability of the phase biaxiality of this mixture [16]. It should also be noticed that lyotropic micellar systems add another complication as they have more than one component and are anyway different in that the shape of the constituent micelles can vary in different regions of the phase diagram [17].

The reason for the failure to date to observe thermotropic biaxial nematics may be connected with the competition between this candidate mesophase and other potential molecular organizations. Thus, if we return to the phase

diagram predicted by purely orientational interactions [12] it seems that only a small region of molecular biaxiality around the maximum stands a chance of being observed before a transition to smectic or crystal steps in [18], very often arising at temperatures some 10% lower that the clearing temperature. To test this type of competition hypothesis theoretical models with full translational freedom rather than lattice models should be employed. As theoretical predictions of phase transitions for off–lattice models are not easily available, the use of computer simulations (see, e.g. [19]) to test the physical implications of a chosen model of molecular interactions becomes particularly important. A pioneering work from this point of view has been that of Allen [20, 21] who examined, using Molecular Dynamics, a system of hard biaxial ellipsoids going from flat–like to rod–like shapes and showed the existence of a biaxial nematic phase [20]. Systems of purely repulsive particles formed of strings of oblate ellipsoids with a repulsive core similar to that of Gay-Berne particles [22] have been studied by Sarman [23] and were also found to give a biaxial nematic.

Hard particle systems are of course not temperature driven and it might be significant that they bear more similarity to colloidal suspensions [24] or to the lyotropic systems where the biaxial nematic was found. The question of the existence of a biaxial nematic in a thermotropic system, especially in competition with the formation of smectics, is thus quite an open one that we wish to address here.

We have considered for this purpose a system of biaxial particles, using a generalized attractive–repulsive Gay–Berne pair potential that we have previously developed [25]. We consider the effect of changing the interaction biaxiality and examine a few cases where shape and interaction biaxiality have the same or opposite sign. We then perform a fairly large scale isobaric–isothermal (NPT) computer simulation for a system of biaxial particles with a selected parameterization and show that it forms biaxial nematic and smectic phases. We characterize the observed biaxial phases in terms of orientational order parameters and a suitable set of averaged Stone [26, 27] rotational invariants.

Our conclusion is that thermotropic biaxial nematics and smectics can exist also for off lattice attractive–repulsive systems in competition with crystalline

phases.

2 Model

We consider a system formed by a set of N identical ellipsoidal biaxial particles interacting with the generalized attractive–repulsive Gay–Berne (GB) interaction [25]

$$\begin{aligned} U(\omega_1,\omega_2,\mathbf{r}_{12}) &= 4\epsilon_0\epsilon(\omega_1,\omega_2,\hat{\mathbf{r}}_{12}) \\ &\times \Big[\Big(\frac{\sigma_c}{r_{12}-\sigma(\omega_1,\omega_2,\hat{\mathbf{r}}_{12})+\sigma_c}\Big)^{12} \\ &\quad -\Big(\frac{\sigma_c}{r_{12}-\sigma(\omega_1,\omega_2,\hat{\mathbf{r}}_{12})+\sigma_c}\Big)^{6}\Big]. \end{aligned} \tag{1}$$

The biaxial ellipsoids have axes σ_x, σ_y, σ_z, orientation ω_i and their center–center intermolecular vector is $\mathbf{r}_{12} = r_{12}\,\hat{\mathbf{r}}_{12}$ with length r_{12} and orientation $\hat{\mathbf{r}}_{12}$, where we use the cap to indicate a unit vector. The potential contains a shape (i.e. anisotropic contact distance) $\sigma(\omega_1,\omega_2,\hat{\mathbf{r}}_{12})$ and an interaction term $\epsilon(\omega_1,\omega_2,\hat{\mathbf{r}}_{12})$, namely

$$\sigma(\omega_1,\omega_2,\hat{\mathbf{r}}_{12}) = (2\,\hat{\mathbf{r}}_{12}^T\mathbf{A}^{-1}(\omega_1,\omega_2)\hat{\mathbf{r}}_{12})^{-1/2}. \tag{2}$$

The symmetric overlap matrix $\mathbf{A}$ is defined as

$$\mathbf{A}(\omega_1,\omega_2) = \mathbf{M}^T(\omega_1)\mathbf{S}^2\mathbf{M}(\omega_1) + \mathbf{M}^T(\omega_2)\mathbf{S}^2\mathbf{M}(\omega_2), \tag{3}$$

where $\mathbf{S}$ is the shape matrix with elements $S_{ab} = \delta_{a,b}\sigma_a$ and $\mathbf{M}(\omega_i)$ are rotation matrices from laboratory to molecular frame i. The interaction term is $\epsilon(\omega_1,\omega_2,\hat{\mathbf{r}}_{12}) = \epsilon^{\nu}(\omega_1,\omega_2)\epsilon'^{\mu}(\omega_1,\omega_2,\hat{\mathbf{r}}_{12})$, with μ and ν empirical exponents [22] and

$$\epsilon(\omega_1,\omega_2) = (\sigma_x\sigma_y+\sigma_z^2)\left[\frac{2\sigma_x\sigma_y}{\det[\mathbf{A}]}\right]^{1/2}, \tag{4}$$

$$\epsilon'(\omega_1,\omega_2,\hat{\mathbf{r}}_{12}) = 2\,\hat{\mathbf{r}}_{12}^T\mathbf{B}^{-1}(\omega_1,\omega_2)\hat{\mathbf{r}}_{12}. \tag{5}$$

The symmetric interaction matrix $\mathbf{B}$ is in turn

$$\mathbf{B}(\omega_1,\omega_2) = \mathbf{M}^T(\omega_1)\mathbf{E}\mathbf{M}(\omega_1) + \mathbf{M}^T(\omega_2)\mathbf{E}\mathbf{M}(\omega_2), \tag{6}$$

where the matrix $\mathbf{E}$ with elements $E_{ab} = \delta_{a,b}(\epsilon_0/\epsilon_{ab})^{1/\mu}$ contains the parameters ϵ_x, ϵ_y and ϵ_z proportional to the well depths for the *side–to–side*, *face–to–face* and *end–to–end* interactions of the molecules. We employ units of distance, σ_0, and energy, ϵ_0, and well width parameter σ_c.
Biaxial mesogens are often characterized by a biaxiality parameter representing deviation from cylindrical symmetry. While this is an all important concept also for the molecular design of new mesogens [28], it is also a loosely defined one. In particular, it should be pointed out that if different molecular interactions contribute significantly to the pair potential then each of them can have a different biaxiality parameter. In our case the deviation from uniaxiality of repulsive and attractive interactions can be concisely described in terms of two parameters:

Shape biaxiality

$$\lambda_\sigma = \sqrt{3/2}\frac{\sigma_x - \sigma_y}{2\sigma_z - \sigma_x - \sigma_y}, \tag{7}$$

Interaction biaxiality

$$\lambda_\epsilon = \sqrt{3/2}\frac{\epsilon_x^{-1/\mu} - \epsilon_y^{-1/\mu}}{2\epsilon_z^{-1/\mu} - \epsilon_x^{-1/\mu} - \epsilon_y^{-1/\mu}}. \tag{8}$$

It is important to notice that these parameters are quite independent and can even have opposite sign. If we consider the interaction potential as two molecules approach with a certain orientation (say with two axes parallel) the position of the energy minimum is clearly linked to the closest approach distance and then on the σ_i and the chosen shape biaxiality. On the other hand the interaction biaxiality λ_ϵ defines the order of the strongest potential wells. In Figures 1 and 2 we see examples of λ_σ and λ_ϵ parameterizations corresponding to different energy profiles. We see that varying the two types of biaxiality, for instance by suitable chemical substitution, can provide an important handle to tuning the intermolecular potential.

2.1 Biaxial Order Parameters

Since we are after the generation of biaxial phases it seems appropriate to briefly discuss the orientational order in such phases, if only to have a way

of monitoring the occurrence or not of phase biaxiality. The description of the static orientational properties can be realized in terms of the first few expansion coefficients of the single particle orientational distribution [29] in a basis of symmetrized Wigner rotation matrices [12, 30] (both phase and molecules have an effective D_{2h} symmetry)

$$R^L_{m,n} = \frac{1}{4}\delta_{L,even}\delta_{m,even}\delta_{n,even}[D^{L*}_{m,n} + D^{L*}_{-m,n} + D^{L*}_{m,-n} + D^{L*}_{-m,-n}]. \quad (9)$$

These second rank order parameters can be explicitly written as

$$\langle R^2_{00}\rangle = \left\langle \frac{3}{2}\cos^2\beta - \frac{1}{2}\right\rangle, \quad (10)$$

$$\langle R^2_{20}\rangle = \left\langle \sqrt{\frac{3}{8}}\sin^2\beta\cos 2\alpha\right\rangle, \quad (11)$$

$$\langle R^2_{02}\rangle = \left\langle \sqrt{\frac{3}{8}}\sin^2\beta\cos 2\gamma\right\rangle, \quad (12)$$

$$\langle R^2_{22}\rangle = \left\langle \frac{1}{4}\left(1+\cos^2\beta\right)\cos 2\alpha\cos 2\gamma - \frac{1}{2}\cos\beta\sin 2\alpha\sin 2\gamma\right\rangle, \quad (13)$$

where α, β and γ are Euler angles [30] giving the orientation of the molecule in the director frame with axes $\hat{\mathbf{X}}$, $\hat{\mathbf{Y}}$ and $\hat{\mathbf{Z}}$. The order parameters are computed from the eigenvalues of the three ordering matrices relative to the $\hat{\mathbf{x}}$, $\hat{\mathbf{y}}$ and $\hat{\mathbf{z}}$ molecular axes [12].

We recall that $\langle R^2_{00}\rangle$ is the standard $\langle P_2\rangle$ order parameter of uniaxial phases while $\langle R^2_{22}\rangle$, which is different from zero only for biaxial molecules in biaxial phases, is the largest and thus most useful biaxial parameter. We shall typically monitor $\langle R^2_{22}\rangle$ as an indicator for phase biaxiality.

3 Monte Carlo Simulations

3.1 Exploring the effect of biaxialities

As we have just discussed, model particles with various combinations of shape and interaction biaxiality can be chosen. This of course means that it would be extremely demanding to perform a systematic study with the aim of exploring all possibilities. We have then chosen to perform a preliminary study

as a guide towards choosing a promising system to investigate with a large scale simulation. The preliminary work has explored the effect of interaction anisotropy on a system with fixed shape biaxiality λ_σ. Thus, we have assumed $\sigma_x = 1.4$, $\sigma_y = 0.714$ and $\sigma_z = 3$ (all in σ_0 units) giving $\lambda_\sigma = 0.216$. The model exponents have been fixed to $\mu = 1$, $\nu = 3$ [31] and also $\sigma_c = \sigma_y$. Several interaction biaxialities have then been explored: (i) $\lambda_\epsilon = 0$ ($\epsilon_x = 1$, $\epsilon_y = 1$ and $\epsilon_z = 0.2$, all in ϵ_0 units); (ii) $\lambda_\epsilon = 0.025$ ($\epsilon_x = 1$, $\epsilon_y = 1.2$ and $\epsilon_z = 0.2$); (iii) $\lambda_\epsilon = 0.042$ ($\epsilon_x = 1$, $\epsilon_y = 1.4$ and $\epsilon_z = 0.2$); and (iv) $\lambda_\epsilon = -0.042$ ($\epsilon_x = 1.4$, $\epsilon_y = 1$ and $\epsilon_z = 0.2$). A uniaxial sample $\lambda_\sigma = 0$, $\lambda_\epsilon = 0$ ($\sigma_x = \sigma_y = 1$, $\sigma_z = 3$, $\epsilon_x = \epsilon_y = 1$ and $\epsilon_z = 0.2$) has also been simulated.

Systems with $N = 1024$ particles under isobaric–isothermal (NPT) conditions [32] have been simulated at various temperatures in a cooling–down sequence of Monte Carlo runs started from well equilibrated configurations in the isotropic phase. We have employed a rectangular box with periodic boundary conditions and director axes parallel to the laboratory frame and set the dimensionless pressure $P^* \equiv \sigma_0^3 P/\epsilon_0 = 8$ allowing the box shape to change with a linear sampling of the volume $V^* \equiv V/\sigma_0^3$. We have adopted a pair potential cutoff radius $r_c = 4\ \sigma_0$, a Verlet neighbor list [33] of radius $r_l = 5\ \sigma_0$, and the acceptance ratio for MC moves has been set to 0.4. Molecular orientations have been stored as quaternions [34, 35]. We have performed the computation of thermodynamic observables sampling one configuration every 20 cycles, one cycle being a random sequence of N attempted MC moves. In Figures 3–a, b we plot the average energy per particle $\langle U^* \rangle = \langle U \rangle/\epsilon_0$ and number density $\langle \rho^* \rangle = N\sigma_0^3 \langle 1/V \rangle$ as a function of temperature $T^* = k_B T/\epsilon_0$ for the four systems (i)–(iv) together with results for the uniaxial case. We notice that the effect of all biaxial perturbations is a shift of the observed values to lower temperatures. The curves for the (i)–(iv) systems also appear more continuous than the uniaxial (e), which presents well identifiable jumps at the isotropic–nematic and even nematic–smectic transformations. To see the nature of the phases obtained we show in Figures 3–c, d a plot of the two main [12] uniaxial and biaxial order parameters $\langle R^2_{00} \rangle$ and $\langle R^2_{22} \rangle$. We see from Figures 3 that all systems produce one or more orientationally ordered phases. Figure 3–d shows that all systems

(except of course the uniaxial) yield some type of biaxial phase at sufficiently low temperatures. The largest effect and clearest biaxial cases appears to be that of pure shape biaxiality (i) and that of shape and interaction biaxialities with opposing sign (iv). We notice, however, that the biaxial phase for the $\lambda_\epsilon = 0$ case (i) occurs at a much lower temperature than the isotropic–nematic transition hinting, as we have verified from our investigation of the structure, that the transformation is from the uniaxial nematic directly to the biaxial smectic phase. Such a low temperature indicates a potential difficulty in realizing a real biaxial nematic purely based on shape anisotropy. This is to some extent true also when allowing for non steric interactions at least for the positive λ_ϵ parameterizations (i) and (iii) but not for the negative interaction biaxiality case (iv). The main finding of our preliminary study is then that parameterizations (i)–(iii) strongly favor *face–to–face* arrangements leading to the formation of biaxial smectic phases in preference to biaxial nematics which were in fact not observed for $\lambda_\epsilon \geq 0$.

3.2 Simulation of a system with opposite shape and interaction biaxialities

To enhance our chances of observing a biaxial nematic we have thus chosen to investigate a system with an even larger negative λ_ϵ than that used in the preliminary study. We recall that physically this corresponds to enhancing lateral attractive interactions between molecules. We have then chosen for our model mesogen particles biaxial GB parameters $\sigma_x = 1.4$, $\sigma_y = 0.714$, $\sigma_z = 3$ for the axes (all in σ_0 units) and $\epsilon_x = 1.7$, $\epsilon_y = 1.2$ and $\epsilon_z = 0.2$ for the interaction strengths (all in ϵ_0 units). Thus, we have shape biaxiality $\lambda_\sigma = 0.216$ and interaction biaxiality $\lambda_\epsilon = -0.06$. We use model exponents $\mu = 1$, $\nu = 3$ and minimum contact distance $\sigma_c = \sigma_y = 0.714\sigma_0$.

We have performed isobaric–isothermal ensemble Monte Carlo simulations of $N = 1024$ and also $N = 8192$ biaxial Gay–Berne particles, using the same conditions adopted for our exploratory runs. In Table 1 we report the temperature T^*, average enthalpy $\langle H^* \rangle = (\langle U \rangle + P\langle V \rangle)/\epsilon_0$, energy $\langle U^* \rangle$ and number density $\langle \rho^* \rangle$ for the $N = 8192$ system. The changes occurring in the thermodynamic quantities upon varying the temperature are essentially

continuous for both system sizes, as we can see from Figures 4–a, b for the energy, number density and estimated transition temperatures. We have then determined orientational order parameters, radial correlation function and related anisotropies, rotational invariants, structural properties that we shall now describe in detail. The full set of order parameters $\langle R^2_{00}\rangle$, $\langle R^2_{02}\rangle$, $\langle R^2_{20}\rangle$ and $\langle R^2_{22}\rangle$ are reported in Table 2 for the $N = 8192$ system and plotted, also for the $N = 1024$ sample, in Figures 5–a, d. The usual second rank order parameter $\langle R^2_{00}\rangle$ shows the onset of the nematic phase at $T^* = 3.2$ but then increases quite regularly all through over the temperature range. In contrast $\langle R^2_{22}\rangle$ shows clearly the occurrence of a uniaxial–biaxial transition at $T^* = 2.9$ (see Figure 5–d). To assess if the phases we are studying are fluid or frozen in some glassy or, at least at the lowest temperatures, crystalline state, we have calculated the mean square displacements $\langle l\rangle_a = \{\sum_i^N \sum_n^M [r^{(n)}_{i,a} - r^{(0)}_{i,a}]^2\}^{1/2}/(NM)$ where $a = X$, Y or Z refers to one of the three director frame axes and $\mathbf{r}^{(n)}_i = \{r_{i,x}, r_{i,y}, r_{i,z}\}^{(n)}$ the i_th particle position with respect to the director frame after n of M MC cycles starting from an arbitrary point $\mathbf{r}^{(0)}_i$. These are plotted in Figure 6 and show that at the uniaxial–biaxial nematic transition the system is still quite fluid according to the classical Lindemann type criterion [36] of comparing $\langle l\rangle_a$ with molecular dimensions, although of course, the system becomes more and more rigid as the temperature is lowered, until at $T^* = 2.75$ we observe the first instance of smectic layering. We notice that in every case the mean square mobility is greater along the principal director axis for this system.

Since we have performed a full simulation study of the system for two sample sizes $N = 1024$ and $N = 8192$, we have plotted both sets of results in Figure 4 and we can see that size effects are quite negligible on energy and density, in agreement with a near or full second–order character of the transformations taking place. This is apparent also from the order parameter plots of Figure 5 where we mainly observe differences in the higher temperature regions due to a better approximation to zero of the order parameter values for the larger system. We notice also that the order parameter $\langle R^2_{20}\rangle$ is very noisy and, since its values are similar to the expected error threshold $O(1/\sqrt{N})$, we observe that it is, differently from $\langle R^2_{22}\rangle$, substantially unreliable as an indicator of phase biaxiality. In Figure 7 we show snapshots of two typi-

cal configurations for the system in the biaxial nematic and biaxial smectic phases. We show lateral and top views of the configurations that give an immediate appreciation of the phase biaxiality, even in the absence of any apparent layering of the nematic system, shown in Figure 7–bottom.

3.3 Structural Properties

Although the orientational order indicates phase biaxiality and the snapshot in Figure 7 are quite suggestive of a biaxial nematic phase we have to check that this assignment is consistent with average (and not just instantaneous) structural properties. Thus, here we turn to a more detailed study of the system structure and to a more reliable classification of the phases obtained. We start calculating the radial correlation function

$$g_0(r) = \frac{1}{4\pi r^2 \rho} \langle \delta(r - r_{12}) \rangle_{12}, \tag{14}$$

where r is the radius of a spherical sampling region and $\langle \ldots \rangle_{12}$ indicates a pair average. In Figure 8 we show $g_0(r)$ and notice, at $T^* = 2.6$, two close and sharp peaks at $r \approx \sigma_y$ and $2\sigma_y$ indicating biaxial packing of nearest neighbor molecules. This pair of peaks is not present at the two other temperatures even at a closer examination (see inset). Notice also that in the nematic phases $g_0(r)$ for the parameterization chosen is somehow intermediate in shape between those typical of an elongated [31] or discotic [37] mesophase. When the system enters a layered structure it is particularly useful to determine the density correlation along the director

$$g(z) = \frac{1}{\pi R^2 \rho} \langle \delta(z - z_{12}) \rangle_{12}, \tag{15}$$

where R is the radius of a cylindrical sampling region and $z_{12} = r_{12} \cos\theta_r$ is measured with respect to the principal Z axis of the director frame, i.e. θ_r is the angle formed by the intermolecular vector $\mathbf{r}_{12}$ and the phase principal director $\hat{\mathbf{Z}}$ [31]. The plot of $g(z)$ shown in Figure 9 indicates clearly the smectic nature of the system at $T^* = 2.6$. This is then a biaxial orthogonal smectic. On the contrary the flat $g(z)$ at temperature $T^* = 2.8$ and 3 are consistent with the homogeneous mass distribution of a nematic structure.

Since the distribution of centers of mass in a liquid crystal is not expected to be isotropic we also compute the anisotropic positional correlation functions

$$g_n^+(r) = \frac{1}{4\pi r^2 \rho} \langle \delta(r - r_{12}) P_n(\cos\theta_r) \rangle_{12}. \tag{16}$$

These $g_n^+(r)$ provide a set of anisotropy coefficients for the distribution of intermolecular vectors with respect to the principal director $\hat{\mathbf{Z}}$ analogous to the orientational order parameters for the distribution of molecular axes with respect to the director frame.

In Figure 10 we report the second rank correlation $g_2^+(r)$. We see once more a peculiarity in the lowest temperature curve where the value, similar to the lowest possible value of $-1/2$, indicates nearly perfect biaxial stacking in the smectic for the first few neighbors, with a structuredness propagating across our sample size. The first positive peak originates from molecules in the nearest layer. The curves at the two other temperatures are essentially identical and only show first neighbor stacking, indicating that the intermolecular vector distribution in the uniaxial and biaxial nematic does not seem to vary.

3.4 Rotational Invariants

A convenient description of the positional–orientational correlations for a system with overall spherical symmetry, as in the case of a system with no external symmetry breaking field applied, can be effected in terms of the expansion coefficients of the pair correlation function

$$g^{(2)}(\omega_1, \omega_2, \mathbf{r}_{12}) = \frac{1}{\rho} \frac{P^{(2)}(\omega_1, \omega_2, \mathbf{r}_{12})}{P^{(1)}(\omega_1) P^{(1)}(\omega_2)}, \tag{17}$$

in an orthogonal basis of rotational invariant functions $S_{n_1 n_2}^{L_1 L_2 L_3}(\omega_1, \omega_2, \hat{\mathbf{r}}_{12})$ as introduced first by Blum and Torruella [26] and later by Stone [27]. Notable examples of the expansion coefficients for biaxial systems are (real parts are shown)

$$S_{00}^{220}(r) = \frac{1}{2\sqrt{5}} \left\langle \delta(r - r_{12}) \left(-1 + 3\,(\hat{\mathbf{z}}_1 \cdot \hat{\mathbf{z}}_2)^2\right) \right\rangle_{12}, \tag{18}$$

$$S_{20}^{220}(r) = \frac{\sqrt{3}}{2 \times \sqrt{10}} \left\langle \delta(r - r_{12}) \left((\hat{\mathbf{x}}_1 \cdot \hat{\mathbf{z}}_2)^2 - (\hat{\mathbf{y}}_1 \cdot \hat{\mathbf{z}}_2)^2 \right) \right\rangle_{12}, \tag{19}$$

$$S_{22}^{220}(r) = \frac{1}{4\times\sqrt{5}}\,\langle\delta(r-r_{12})\,(\quad (\hat{\mathbf{x}}_1\cdot\hat{\mathbf{x}}_2)^2 - (\hat{\mathbf{x}}_1\cdot\hat{\mathbf{y}}_2)^2 - (\hat{\mathbf{y}}_1\cdot\hat{\mathbf{x}}_2)^2 + (\hat{\mathbf{y}}_1\cdot\hat{\mathbf{y}}_2)^2 - 2\,(\hat{\mathbf{x}}_1\cdot\hat{\mathbf{y}}_2)\,(\hat{\mathbf{y}}_1\cdot\hat{\mathbf{x}}_2) - 2\,(\hat{\mathbf{x}}_1\cdot\hat{\mathbf{x}}_2)\,(\hat{\mathbf{y}}_1\cdot\hat{\mathbf{y}}_2)\;)\rangle_{12}\,, \qquad (20)$$

where $\hat{\mathbf{x}}_i$, $\hat{\mathbf{y}}_i$, $\hat{\mathbf{z}}_i$ are unit vectors defining the orientations of molecular axes and r is the radius of a spherical sampling region. The average invariants can be written for large separations (compared to molecular dimensions) $r \gg \sigma_c$ in terms of single particle order parameters

$$S_{00}^{220}(r) = \frac{1}{\sqrt{5}}\left(\langle R_{00}^2\rangle^2 + 2\langle R_{20}^2\rangle^2\right), \qquad (r\gg\sigma_c) \qquad (21)$$

$$S_{20}^{220}(r) = \frac{1}{\sqrt{5}}\left(\langle R_{00}^2\rangle\langle R_{02}^2\rangle + 2\langle R_{20}^2\rangle\langle R_{22}^2\rangle\right), \qquad (r\gg\sigma_c) \qquad (22)$$

$$S_{22}^{220}(r) = \frac{1}{\sqrt{5}}\left(\langle R_{02}^2\rangle^2 + 2\langle R_{22}^2\rangle^2\right). \qquad (r\gg\sigma_c) \qquad (23)$$

This asymptotic behavior provides a useful route to check the single particle order parameters obtained earlier on, even if these equations do not depend on the sign of each order parameter. We have calculated these average Stone invariants and in Figures 11, 12 and 13 we report results for $S_{00}^{220}(r)$, $S_{20}^{220}(r)$ and $S_{22}^{220}(r)$ at three temperatures. We see that the Stone invariants also confirm the biaxiality of the two lower temperature phases. The order parameters obtained analyzing the large separation plateau are consistent with those obtained by simultaneous diagonalization of the three order matrices (see Table 2). The curves are not very structured and the limit plateau of the correlations, when present, is reached after 5–6 σ_0 units.

4 Conclusions

We have presented a computer simulation study of an anisotropic system of elongated particles with both shape and attractive interaction biaxiality and showed that it produces biaxial phases. We have found that while positive biaxialities in both shape and interaction favor biaxial stacking, they also favor too much the formation of smectic layering. On the other hand, we

have found that a negative interaction biaxiality λ_ϵ yields a stable and fairly wide biaxial nematic, that we have confirmed with a variety of observables. At lower temperature an upright biaxial smectic phase is obtained, that to our knowledge, has also still to be experimentally found [1]. In practice, a negative attraction biaxiality could be obtained by lateral groups (e.g. weak hydrogen bonding sites) that favor *side–to–side* attraction, thus competing with *face–to–face* stacking. The present findings should hopefully be of help in the current effort towards designing mesogenic molecules that can yield a thermotropic biaxial nematic phase.

Acknowledgments

We thank MURST *PRIN Cristalli Liquidi*, CNR *PF MSTA–II*, University of Bologna, EU *TMR* contract FMRX–CT97–0121 and NEDO (Japan) for financial support.

References

[1] see, e.g. Oxford Workshop on Biaxial Nematics, ed. D. Bruce, G.R. Luckhurst and D. Photinos, Mol. Cryst. Liq. Cryst. **323**, 153 (1998).

[2] see, e.g., (a) Liquid Crystals for Advanced Technologies (Proc. Materials Research Society Symposia), edited by T.J. Bunning, **425**, (1996); (b) Liquid Crystal Materials, Devices and Displays (Proc. SPIE), edited by R. Shashidhar, (1995).

[3] M.J. Freiser, Phys. Rev. Lett. **24**, 1041 (1970).

[4] S.M. Fan, I.D. Fletcher, B. Gündoḡan, N.J. Heaton, G. Kothe, G.R. Luckhurst and K. Praefcke, Chem. Phys. Lett. **204**, 517 (1993).

[5] J.R. Hughes, G. Kothe, G.R. Luckhurst, J. Malthète, M.E. Neubert, I. Shenouda, B.A. Timimi and M. Tittelbach, J. Chem. Phys. **107**, 9252 (1997).

[6] J.P. Straley, Phys. Rev. A **10**, 1881 (1974).

[7] R.G. Priest, Solid State Comm. **17**, 519 (1975).

[8] G.R. Luckhurst, C. Zannoni, P.L. Nordio and U. Segre, Mol. Phys., **30**, 1345 (1975).

[9] D.K. Remler and A.D.J Haymet, J. Phys. Chem. **90**, 5426 (1986).

[10] B. Bergensen, P. Palffy–Muhoray and D. Dunmur, Liq. Cryst. **3**, 347 (1988).

[11] G.R. Luckhurst and S. Romano, Mol. Phys. **40**, 129 (1980).

[12] F. Biscarini, C. Chiccoli, F. Semeria, P. Pasini and C. Zannoni, Phys. Rev. Lett. **75**, 1803 (1995).

[13] (a) S. Chandrasekhar, Contemp. Phys. **29**, 527 (1988); (b) J. Malthête, L. Liébert, A.M. Levelut and Y. Galerne, C. R. Acad. Sc. Paris **303**, 1073 (1986); (c) K. Praefcke, B. Kohne, B. Gündoḡan, D. Singer, D. Demus, S. Diele, G. Pelzl and U. Bakow, Mol. Cryst. Liq. Cryst. **198**, 393 (1991); (d) J-F. Li, V. Percec, C. Rosenblatt and O.D. Lavrentovich, Europhys. Lett. **25**, 199 (1994).

[14] F. Hessel and H. Finkelmann, Polymer Bulletin **15**, 349 (1986).

[15] L.J. Yu and A. Saupe, Phys. Rev. Lett. **45**, 1000 (1980).

[16] V. Berejnov, V. Cabuil, R. Perzynski and Yu. Raikher, J. Phys. Chem. B **102**, 7132 (1998).

[17] V.L. Lorman, E.A. Oliveira and B. Mettout, Physica B **262**, 55 (1999).

[18] A. Ferrarini, P.L. Nordio, E. Spolaore and G.R. Luckhurst, J. Chem. Soc. Faraday Trans. **91**, 3177 (1995).

[19] *Advances in the Computer Simulations of Liquid Crystals*, edited by P. Pasini and C. Zannoni, (Kluwer Academic Publishers, Dordrecht, 1999).

[20] M.P. Allen, Mol. Phys. **52**, 717 (1984); *ibid.*, Liq. Cryst. **8**, 499 (1990).

[21] P.J. Camp and M.P. Allen, J. Chem. Phys. **106**, 6681 (1997).

[22] J.G. Gay and B.J. Berne, J. Chem. Phys. **74**, 3316 (1981).

[23] S. Sarman, J. Chem. Phys. **104**, 342 (1996); *ibid* J. Chem. Phys. **107**, 3144 (1997).

[24] W.M. Gelbart and A. Ben–Shaul, J. Phys. Chem. **100**, 13169 (1996).

[25] R. Berardi, C. Fava and C. Zannoni, Chem. Phys. Lett. **236**, 462, (1995); *ibid.*, Chem. Phys. Lett. **297**, 8 (1998).

[26] L. Blum and A.J. Torruella, J. Chem. Phys. **56**, 303 (1972).

[27] A.J. Stone, Molec. Phys. **36**, 241 (1978).

[28] K. Praefcke, D. Blunk, D. Singer, J.W. Goodby, K.J. Toyne, M. Hird, P. Styring and W.D.J.A. Norbert, Mol. Cryst. Liq. Cryst. **323**, 231 (1998).

[29] C. Zannoni, in *The Molecular Physics of Liquid Crystals*, chap. 3, edited by G.R. Luckhurst and G.W. Gray (Academic Press, London, 1979).

[30] M.E. Rose, *Elementary Theory of Angular Momentum*, (Wiley, New York, 1957).

[31] R. Berardi, A.P.J. Emerson, and C. Zannoni, J. Chem. Soc. Faraday Trans. **89**, 4069 (1993).

[32] D. Frenkel and B. Smit, *Understanding Molecular Simulation: from Algorithms to Applications*, (Academic Press, San Diego, 1996).

[33] M.P. Allen and D.J. Tildesley, *Computer Simulation of Liquids*, (Clarendon Press, Oxford, 1987).

[34] C. Zannoni and M. Guerra, Mol. Phys. **44**, 849 (1981).

[35] S.L. Altmann, *Rotations, Quaternions, and Double Groups*, (Clarendon Press, Oxford, 1986).

[36] F.H. Stillinger, Science **267**, 1935 (1995).

[37] M. Bates and G.R. Luckhurst, J. Chem. Phys. **104**, 6696 (1996).

T^*	N_e	N_p	$\langle H^* \rangle$	$\langle U^* \rangle$	$\langle \rho^* \rangle$
2.60	60	120	6.824 ± 0.090	-16.293 ± 0.073	0.346 ± 0.001
2.65	600	360	6.790 ± 0.095	-16.333 ± 0.065	0.346 ± 0.002
2.70	150	540	14.725 ± 0.181	-10.470 ± 0.139	0.318 ± 0.002
2.75	380	440	16.510 ± 0.214	-9.198 ± 0.152	0.311 ± 0.002
2.80	20	420	19.674 ± 0.165	-6.987 ± 0.100	0.300 ± 0.001
2.85	20	240	20.843 ± 0.138	-6.265 ± 0.089	0.295 ± 0.001
2.90	223	350	21.655 ± 0.123	-5.793 ± 0.084	0.291 ± 0.001
3.00	20	133	23.034 ± 0.104	-5.030 ± 0.072	0.285 ± 0.001
3.10	24	266	24.430 ± 0.120	-4.281 ± 0.066	0.279 ± 0.001
3.20	100	440	26.059 ± 0.143	-3.435 ± 0.082	0.271 ± 0.001
3.25	20	80	26.990 ± 0.112	-2.958 ± 0.045	0.267 ± 0.001
3.30	80	300	27.251 ± 0.104	-2.860 ± 0.049	0.266 ± 0.001
3.40	40	140	27.829 ± 0.083	-2.639 ± 0.047	0.263 ± 0.001
3.50	20	60	28.322 ± 0.056	-2.468 ± 0.037	0.260 ± 0.001
3.60	20	80	28.737 ± 0.093	-2.338 ± 0.045	0.257 ± 0.001
3.70	20	40	29.163 ± 0.077	-2.206 ± 0.037	0.255 ± 0.001

Table 1: The temperature T^*, average enthalpy $\langle H^* \rangle$ and energy $\langle U^* \rangle$ per particle and number density $\langle \rho^* \rangle$ for the system of $N = 8192$ biaxial GB particles with biaxialities $\lambda_\sigma = 0.216$ and $\lambda_\epsilon = -0.06$. All averages were computed sampling one configuration each 20 MC cycles over NPT production runs (of length N_p k–cycles) at pressure $P^* = 8$. The equilibration runs length N_e and the root mean square errors are also reported.

T^*	$\langle R^2_{00} \rangle$	$\langle R^2_{20} \rangle$	$\langle R^2_{02} \rangle$	$\langle R^2_{22} \rangle$
2.60	0.964 ± 0.001	0.006 ± 0.001	0.006 ± 0.001	0.466 ± 0.001
2.65	0.965 ± 0.003	0.006 ± 0.001	0.006 ± 0.001	0.469 ± 0.001
2.70	0.899 ± 0.004	0.017 ± 0.001	0.019 ± 0.001	0.354 ± 0.005
2.75	0.871 ± 0.005	0.020 ± 0.001	0.024 ± 0.001	0.314 ± 0.008
2.80	0.783 ± 0.005	0.029 ± 0.003	0.039 ± 0.002	0.218 ± 0.014
2.85	0.748 ± 0.008	0.022 ± 0.002	0.042 ± 0.002	0.131 ± 0.008
2.90	0.717 ± 0.010	0.020 ± 0.005	0.045 ± 0.002	0.098 ± 0.020
3.00	0.653 ± 0.011	0.006 ± 0.003	0.050 ± 0.002	0.017 ± 0.008
3.10	0.535 ± 0.012	0.011 ± 0.006	0.058 ± 0.002	0.017 ± 0.007
3.20	0.329 ± 0.032	0.009 ± 0.008	0.057 ± 0.004	0.009 ± 0.006
3.25	0.062 ± 0.020	0.009 ± 0.012	0.021 ± 0.006	0.005 ± 0.004
3.30	0.078 ± 0.033	0.015 ± 0.014	0.021 ± 0.009	0.008 ± 0.005
3.40	0.033 ± 0.018	0.010 ± 0.011	0.011 ± 0.008	0.005 ± 0.003
3.50	0.026 ± 0.014	0.011 ± 0.008	0.010 ± 0.008	0.006 ± 0.003
3.60	0.021 ± 0.009	0.008 ± 0.008	0.005 ± 0.005	0.005 ± 0.003
3.70	0.021 ± 0.011	0.009 ± 0.008	0.007 ± 0.006	0.006 ± 0.004

Table 2: The average biaxial second rank orientational order parameters $\langle R^2_{00} \rangle$, $\langle R^2_{20} \rangle$, $\langle R^2_{02} \rangle$ and $\langle R^2_{22} \rangle$ for the system of $N = 8192$ biaxial GB particles with biaxialities $\lambda_\sigma = 0.216$ and $\lambda_\epsilon = -0.06$ (see Table 1 for computational details).

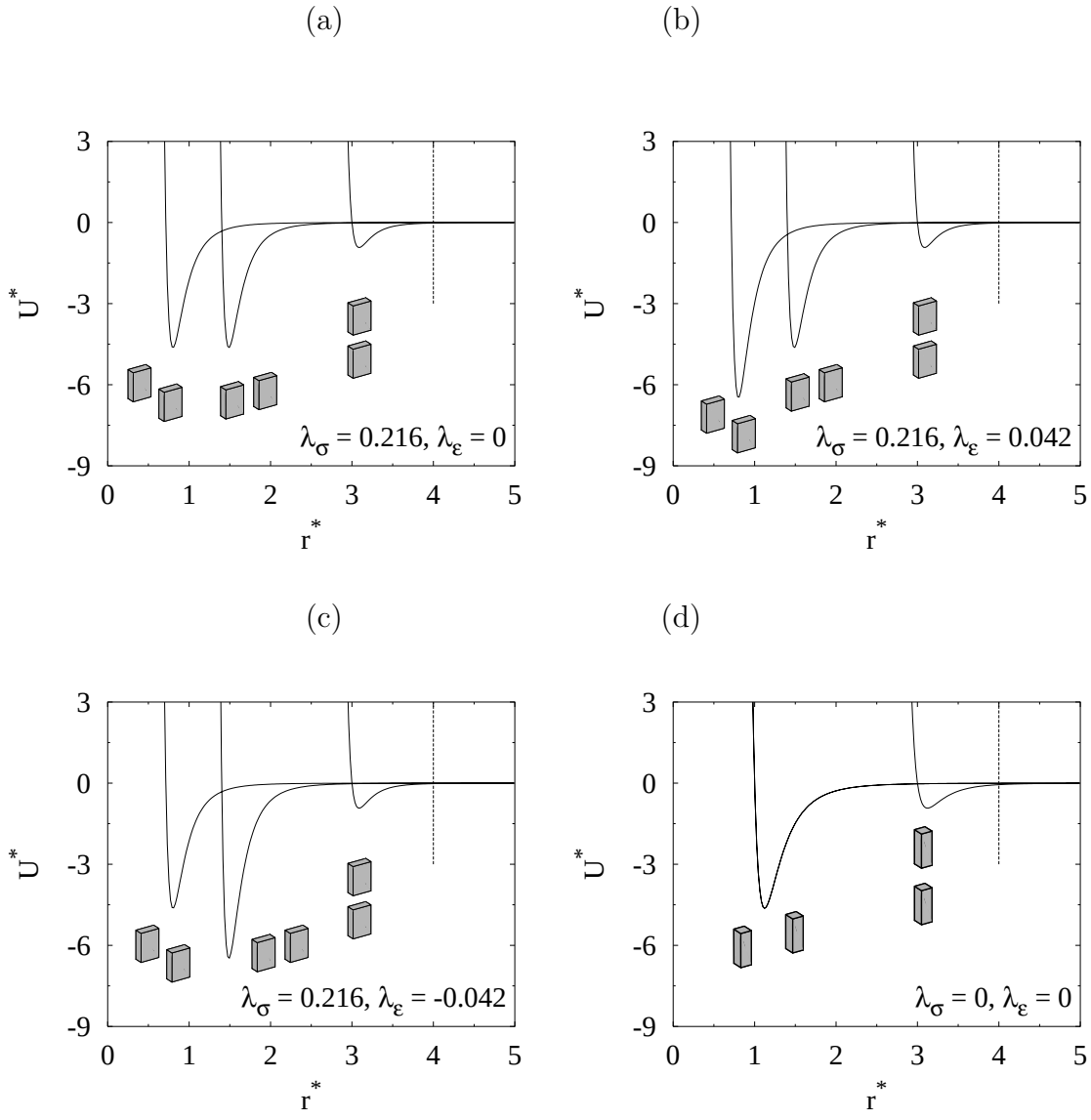

Figure 1: Distance dependence of the $U^* = U/\epsilon_0$ energy for a pair of biaxial Gay–Berne molecules with fixed *face–to–face*, *side–by-side* and *end–to–end* relative configurations using the parameterizations described in the text which corresponding to shape biaxiality $\lambda_\sigma = 0.216$ and interaction biaxiality (a) $\lambda_\epsilon = 0$, (b) $\lambda_\epsilon = 0.042$, and (c) $\lambda_\epsilon = -0.042$. The uniaxial profile with $\lambda_\sigma = 0$ and $\lambda_\epsilon = 0$ is also shown (d). The potential cutoff radius $r_c^* = r_c/\sigma_0 = 4$ is also shown as a vertical dashed segment.

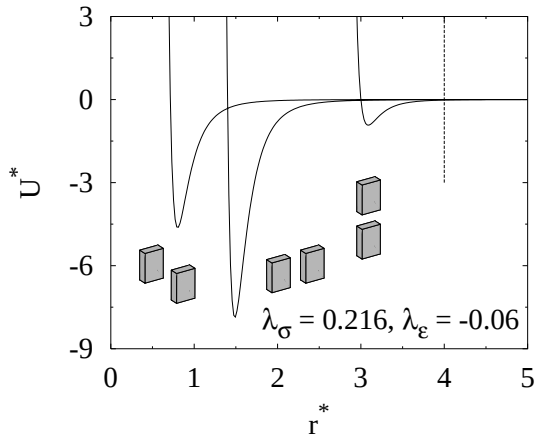

Figure 2: Distance dependence of the biaxial Gay–Berne U^* energy for the parameterization described in the text corresponding to shape biaxiality $\lambda_\sigma = 0.216$ and interaction biaxiality $\lambda_\epsilon = -0.06$. (see Figure 1 for additional details).

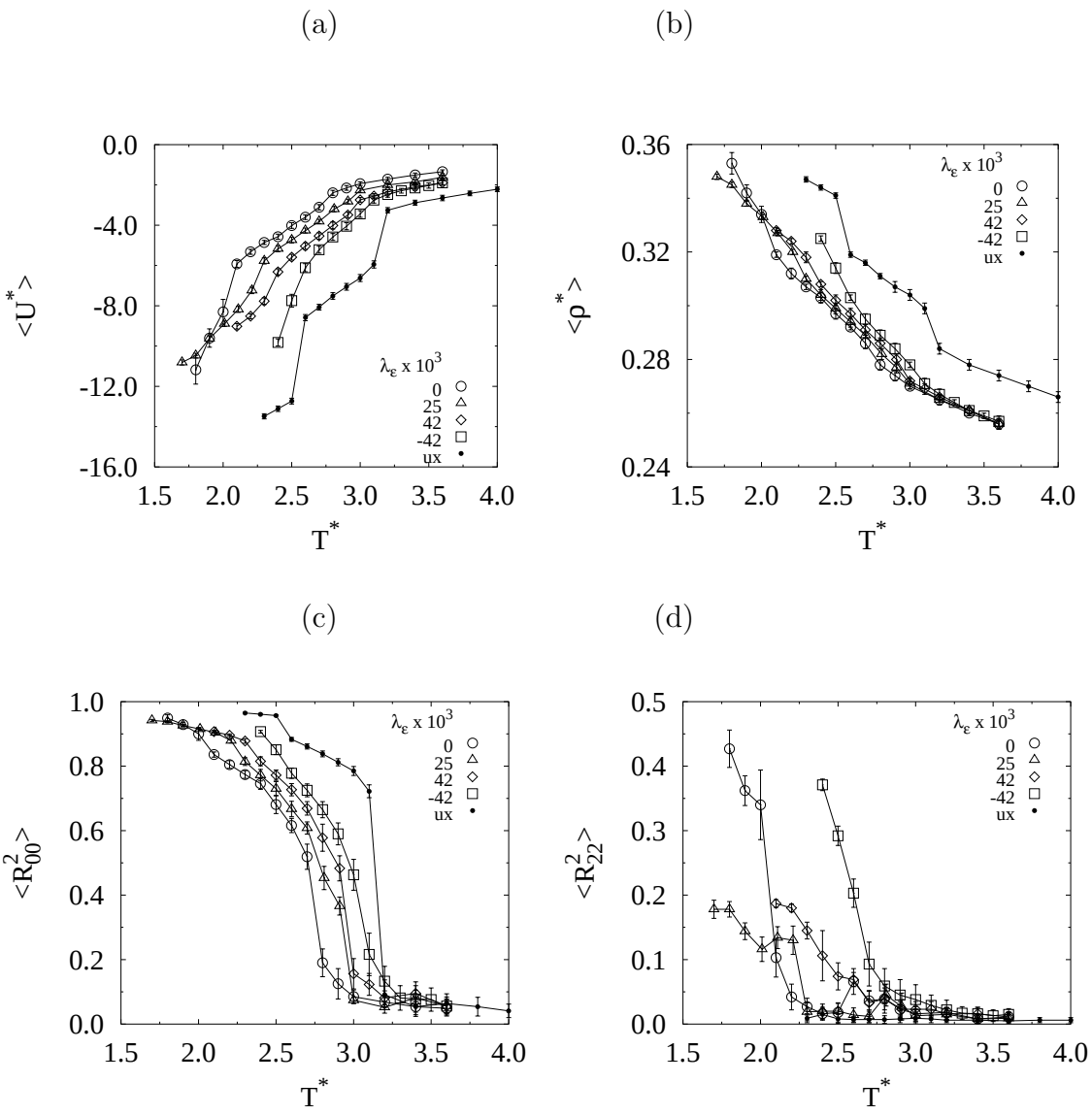

Figure 3: Average energy per particle $\langle U^* \rangle$ (a), number density $\langle \rho^* \rangle$ (b), orientational order parameters $\langle R^2_{00} \rangle$ (c) and $\langle R^2_{22} \rangle$ (d) for systems of $N = 1024$ elongated GB particles with shape biaxiality $\lambda_\sigma = 0.216$ and interaction biaxialities $\lambda_\epsilon = 0$ (circles), 0.025 (triangles), 0.042 (diamonds) and -0.042 (squares) (see Figure 1). Results for a uniaxial system $\lambda_\sigma = \lambda_\epsilon = 0$ (dots) are also shown. All MC simulations were run in the NPT ensemble at $P^* = 8$.

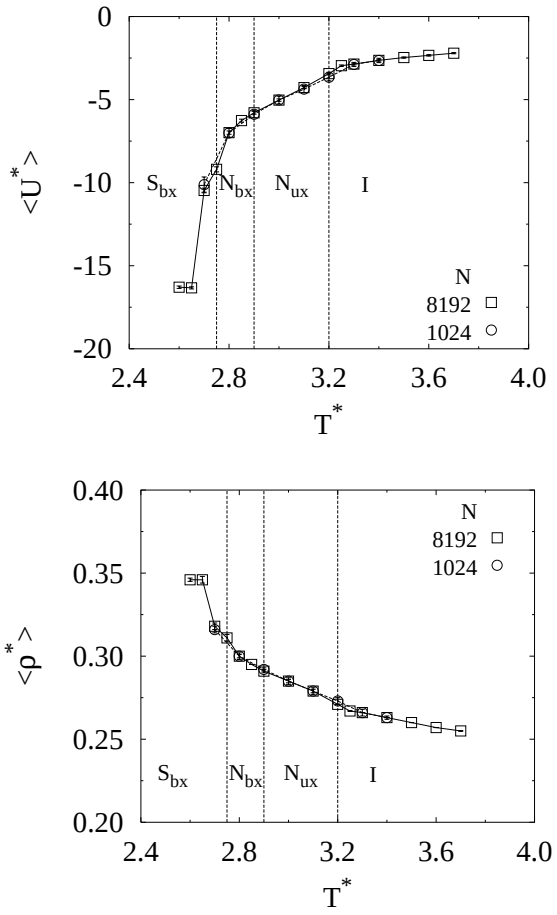

Figure 4: Average energy per particle $\langle U^* \rangle$ (top) and density $\langle \rho^* \rangle$ (bottom) for systems of $N = 1024$ (circles) and $N = 8192$ (squares) biaxial GB particles with biaxialities $\lambda_\sigma = 0.216$ and $\lambda_\epsilon = -0.06$ simulated in the MC–NPT ensemble at $P^* = 8$. The estimated transition temperatures between the isotropic (I), uniaxial nematic (N_{ux}), biaxial nematic (N_{bx}) and biaxial smectic (S_{bx}) phases are shown as dashed vertical lines.

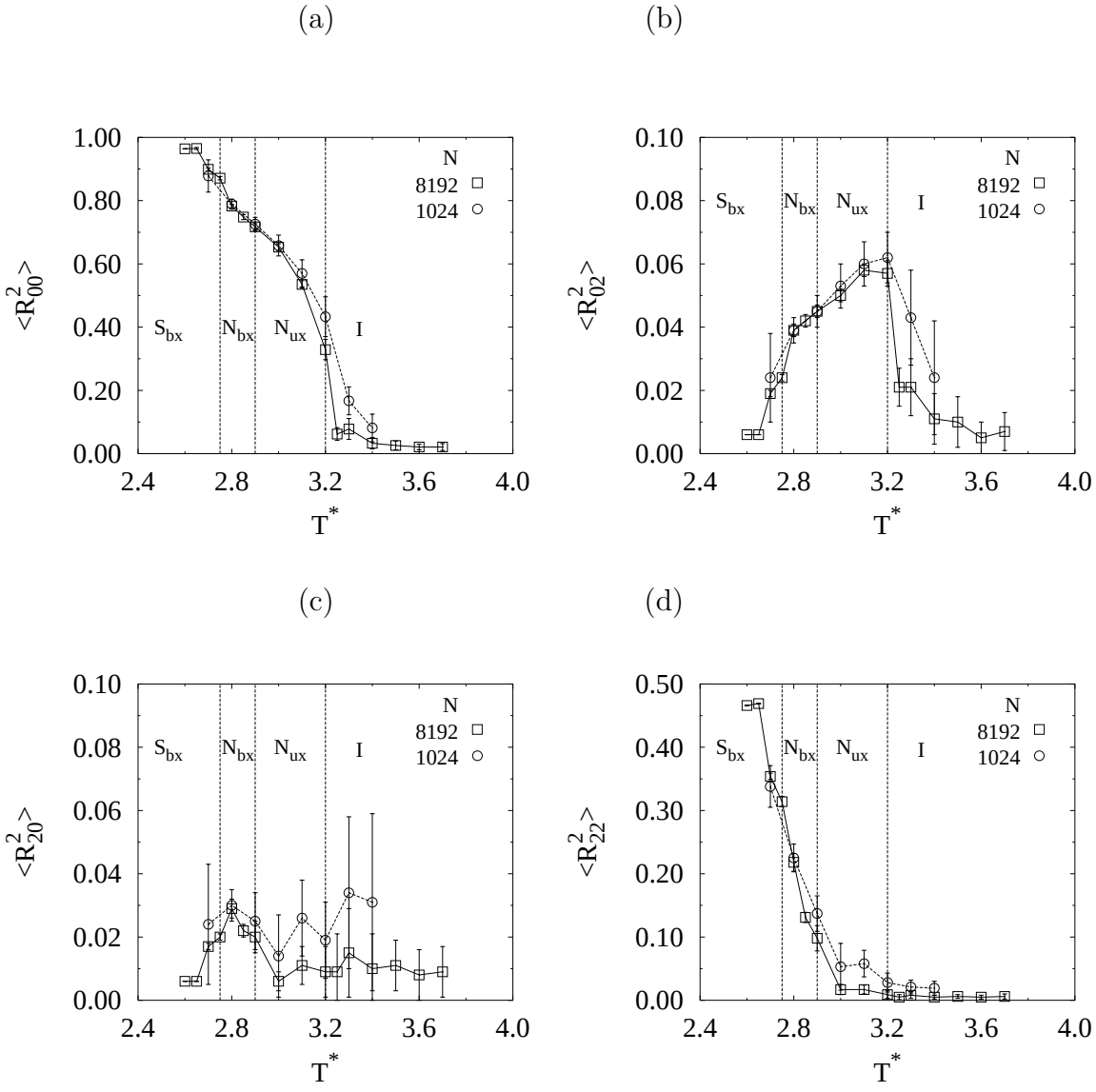

Figure 5: Average orientational order parameters $\langle R^2_{00}\rangle$ (a), $\langle R^2_{02}\rangle$ (b), $\langle R^2_{20}\rangle$ (c) and $\langle R^2_{22}\rangle$ (d) for the systems of $N = 1024$ (circles) and $N = 8192$ (squares) biaxial GB particles of Figure 4.

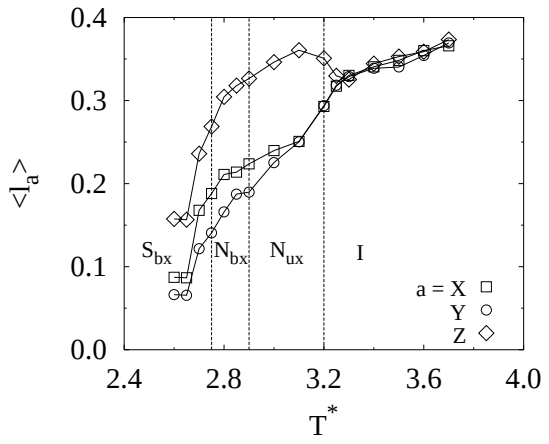

Figure 6: Average molecular mean square displacement $\langle l \rangle_a$ along the $a = X$ (squares), Y (circles) or Z (diamonds) axes of the director frame for the system of $N = 8192$ biaxial GB particles of Figure 4.

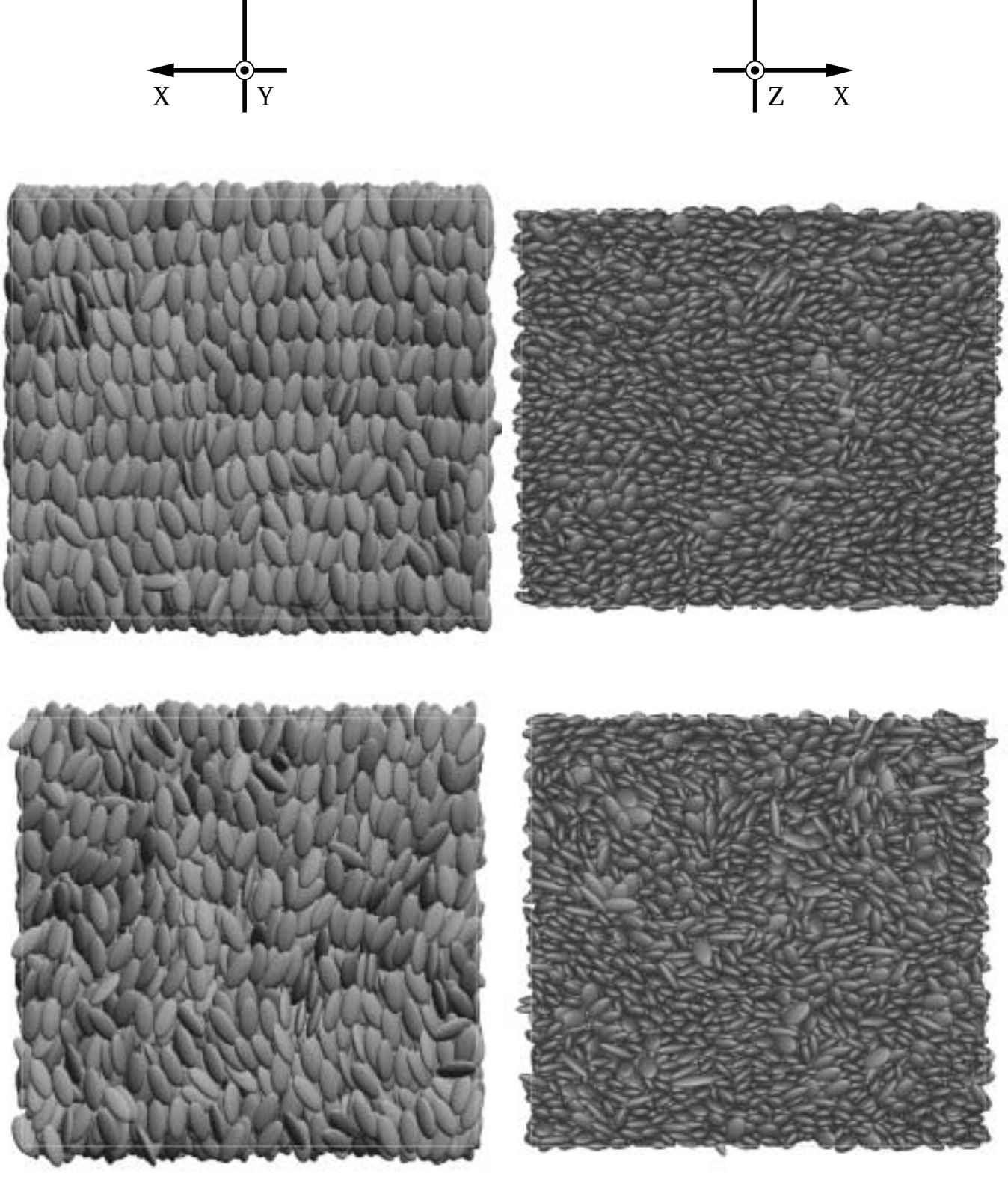

Figure 7: Snapshots of typical MC configurations for the system of $N = 8192$ elongated biaxial GB particles with biaxialities $\lambda_\sigma = 0.216$ and $\lambda_\epsilon = -0.06$. Views from the Y (left) and Z (right) directions of the director frame for the biaxial smectic ($T^* = 2.7$, top) and biaxial nematic ($T^* = 2.8$, bottom) phases are shown.

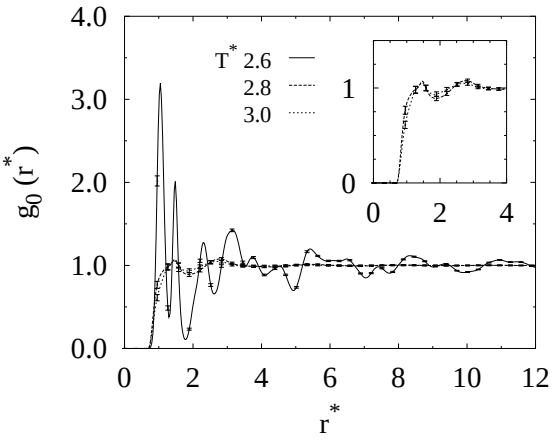

Figure 8: Radial correlation function $g_0(r)$ for the system of $N = 8192$ biaxial GB particles with biaxialities $\lambda_\sigma = 0.216$ and $\lambda_\epsilon = -0.06$ from MC–NPT simulations at $P^* = 8$ and $T^* = 2.6$ (biaxial smectic), 2.8 (biaxial nematic) and 3.0 (uniaxial nematic).

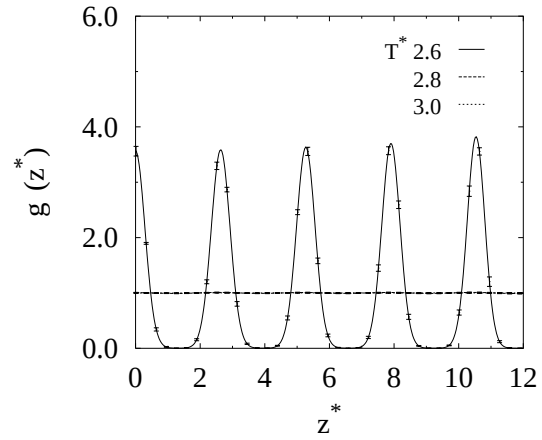

Figure 9: Density correlation along the director $g(z)$ for the system of $N = 8192$ biaxial GB particles of Figure 8.

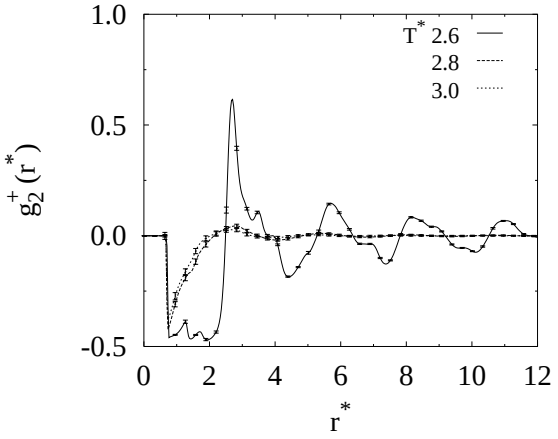

Figure 10: Second rank anisotropic positional correlation $g_2^+(r)$ for the system of $N = 8192$ biaxial GB particles of Figure 8.

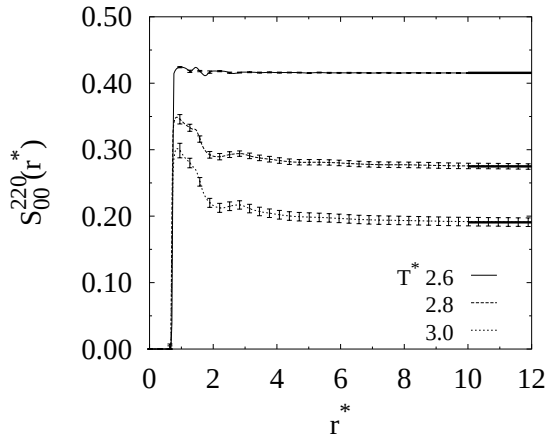

Figure 11: Average orientational correlation $S_{00}^{220}(r)$ for the system of $N = 8192$ biaxial GB particles of Figure 8. The asymptotic values computed from the second rank order parameters are shown as thick horizontal segments.

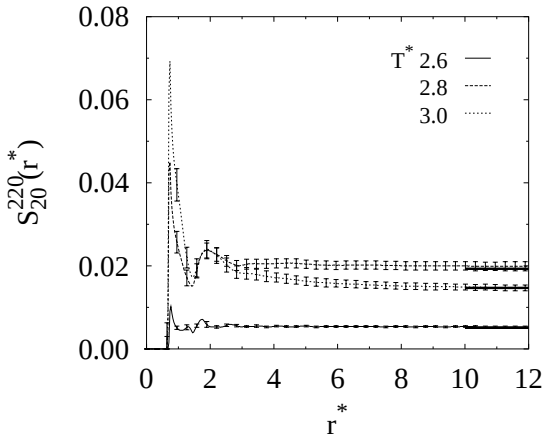

Figure 12: Average orientational correlation $S_{20}^{220}(r)$ for the system of $N = 8192$ biaxial GB particles of Figure 8. The asymptotic values computed from the second rank order parameters are shown as thick horizontal segments.

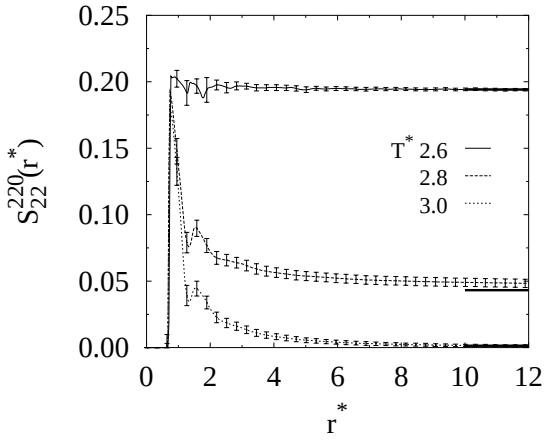

Figure 13: Average orientational correlation $S_{22}^{220}(r)$ for the system of $N = 8192$ biaxial GB particles of Figure 8. The asymptotic values computed from the second rank order parameters are shown as thick horizontal segments.